

# Lawrence Berkeley National Laboratory

## LBL Publications

### Title

Fouling propensity of a poly(vinylidene fluoride) microfiltration membrane to several model oil/water emulsions

### Permalink

<https://escholarship.org/uc/item/962899tr>

### Authors

He, Zhengwang  
Miller, Daniel J  
Kasemset, Sirirat  
et al.

### Publication Date

2016-09-01

### DOI

10.1016/j.memsci.2016.04.018

Peer reviewed

**Fouling propensity of a poly(vinylidene) fluoride microfiltration membrane to several model oil/water emulsions**

**Zhengwang He, Daniel J. Miller<sup>1</sup>, Sirirat Kasemset<sup>2</sup>, Lu Wang, Donald R. Paul, Benny D. Freeman\***

Department of Chemical Engineering, Center for Energy and Environmental Resources, and Texas Materials Institute, The University of Texas at Austin, 10100 Burnet Road Building 133, Austin, TX 78758

\*Corresponding author (Tel: +1-512-232-2803; Email: [freeman@che.utexas.edu](mailto:freeman@che.utexas.edu))

1. Current address: Joint Center for Artificial Photosynthesis, Lawrence Berkeley National Laboratory, 1 Cyclotron Road, Berkeley CA 94702
2. Current address: Evonik Corporation, 4201 Evonik Road, Theodore, AL 36582

Manuscript prepared for submission to the *Journal of Membrane Science*

## **ABSTRACT**

Laboratory membrane fouling studies are often performed with a single foulant. However, studies comparing the behavior of different foulants using a single membrane are rarely reported. In this study, a poly(vinylidene fluoride) (PVDF) microfiltration membrane was challenged with a series of aqueous-based model fouling media, including a suspension of latex beads, as well as soybean, motor and crude oil emulsions, in constant permeate flux fouling experiments. The critical and threshold fluxes were determined for each membrane-foulant pair. Constant permeate flux crossflow fouling experiments were performed at both low and high fluxes. A direct comparison of the fouling propensity of the PVDF membrane to the four fouling media was made. The fouling propensity was evaluated based on threshold flux values and the extent of transmembrane pressure (TMP) increase during constant permeate flux fouling experiments. In this study, the zeta potential of various fouling media correlated with their fouling propensities. The higher the zeta potential, the lower the fouling propensity. The fouling propensity followed the order of: latex beads < soybean oil < crude oil < motor oil. A three-stage TMP profile was observed with high fouling media, such as motor and crude oil emulsions. The TMP increased slowly in the early stage, then increased abruptly, and eventually reached a new pseudo-steady state TMP.

## **HIGHLIGHTS**

1. Fouling by latex bead suspension and soybean, motor and crude oil emulsions was studied.
2. Critical and threshold fluxes were determined using the flux-stepping technique.
3. Fouling propensity was directly related to foulant zeta potential.

## **KEYWORDS**

Fouling propensity, oil emulsion, microfiltration, threshold flux, zeta potential

## 1. INTRODUCTION

Fresh water availability and oilfield wastewater disposal can pose substantial challenges to hydraulic fracturing, and both could be at least partially addressed by recycling and reusing oilfield wastewater [1]. However, wastewater decontamination is required to meet the water quality criteria for reuse. Existing technologies for wastewater treatment, such as the American Petroleum Institute (API) gravity separator, may not be able to sufficiently remove contaminants for further applications or are economically unfavorable [1, 2]. Compared with conventional wastewater treatment, membrane processes are energy efficient, have low capital cost, and have a small footprint [3-9]. However, a great challenge for such membrane processes is membrane fouling, especially when separating complex mixtures [5].

In many published fouling studies, one model foulant is selected to represent a type of foulant mixture. For example, latex beads and silica particles are popular for representing solid particles [10, 11]. Aqueous dodecane and soybean oil emulsions have been used to represent oil/water emulsions [3, 12]. Bovine serum albumin and bacteria suspensions are commonly used to represent proteins and microorganisms in biofouling [13].

Studies with model foulants provide insight into fouling mechanisms for that particular foulant. However, fouling behavior may be unique for every membrane-foulant combination. Foulant properties, such as hydrophobicity, surface charge and concentration, influence membrane fouling behavior, so fouling behavior could vary substantially depending on the foulant. Although fouling studies involving more than one type of model foulant are reported, there are few direct comparisons of multiple model foulants performed on the same membrane and at the same operating conditions. Koo *et*

*al.* developed a constant flux apparatus for modified fouling index (MFI) measurement [11]. They used colloidal silica particles of different sizes. The underlying assumption for the MFI concept was that the cake filtration mechanism applied. To satisfy this assumption, non-deformable colloidal silica particles, which were completely rejected by the membrane, were used in reverse osmosis and nanofiltration fouling experiments. The fouling index varied with particle size [11]. Field *et al.* proposed the critical, threshold, and sustainable flux concepts based on yeast cell suspensions and dodecane-in-water emulsion filtration tests, but direct comparison of the two foulants was not reported [3, 14]. Howe *et al.* collected natural waters from five sources and used a three-step filtration process (prefiltration, fractionation, and fouling determination). However, the focus of their study was to decouple fouling caused by different foulants, including particulates, colloids, dissolved molecular material, and inorganic matter, rather than profiling fouling behavior with respect to different feeds [15].

In this study, poly(vinylidene fluoride) (PVDF) microfiltration (MF) membranes were challenged with a series of four aqueous-based model fouling media, including a suspension of latex beads, as well as soybean, motor and crude oil emulsions. We selected a rather large-pore MF (i.e., 0.2  $\mu\text{m}$ ) membrane, so the organic rejection values were not very high. However, this selection allows one to more quantitatively observe foulant-specific rejection properties and to characterize fouling behavior over an extended time period. These fouling experiments were conducted at the same operating conditions using the same membrane, thereby helping isolate the effects of foulant properties on membrane fouling behavior. Critical and threshold fluxes were determined for each fouling medium using the flux-stepping technique [10, 12]. Membrane fouling

behavior in constant permeate flux crossflow filtration experiments was evaluated at two fluxes.

## **2. MATERIALS AND METHODS**

### **2.1 Materials**

Hydrophobic PVDF microfiltration membranes of 0.2 micron nominal pore rating were kindly supplied by Pall Corporation (Port Washington, NY). Dry flat sheet membrane was received in rolls. To wet the pores, membranes were pretreated by soaking in ethanol for 1 hour and then at least 1 hour of soaking in ultrapure water prior to all experiments. This particular hydrophobic PVDF membrane is commonly used in protein detections [16].

A latex microsphere suspension (5320A) containing 10 wt% polystyrene particles (3.2  $\mu\text{m}$  in diameter) was purchased from Thermo Scientific, Inc. (Fremont, CA). The suspension was stabilized with proprietary ionic and non-ionic surfactants by the manufacturer. The coefficient of variation of particle size was  $\leq 5\%$ , so the suspension had a narrow particle size distribution. Wesson soybean oil was purchased from a local supermarket. Non-detergent motor oil (VV265) was purchased from Ashland Chemical (Lexington, KY). The motor oil contains more than 80% heavy paraffinic distillate. Light crude oil was generously provided by American Refining Group (Bradford, PA). Sodium chloride of analytical grade, anhydrous calcium chloride, ionic strength adjustment solution (1M KCl), pH=6 buffer, sodium hydroxide solution (1 M), hydrochloric acid solution (1 M), and Triton<sup>™</sup> X-100 non-ionic surfactant were purchased from Sigma Aldrich (St. Louis, MO). Xiameter<sup>®</sup> OFX-0193, a silicone-based non-ionic surfactant, was purchased from Dow Corning Corporation (Midland, MI). The chemical structures

of the two surfactants are shown in Supporting Information Figure S - 1. Denatured ethanol and 1 N sodium hydroxide solution were purchased from Fisher Scientific (Fairlawn, NJ). Ultrapure water (18.2M $\Omega$ -cm and 5.4 ppb TOC) was generated by a Millipore RiOS and A10 water purification system (Billerica, MA).

## 2.2 Membrane characterization

The pure water permeance of the PVDF membrane was tested in UHP-76 stirred cells (Sterlitech, Kent, WA) under constant transmembrane pressure. The experimental setup is described in detail in the Supporting Information. The water permeance,  $P$ , is:

$$P = \frac{J}{TMP} \quad [1]$$

where  $J$  is pure water flux, and  $TMP$  is transmembrane pressure.

Sessile drop contact angle was measured with ultrapure water using a Model 200 goniometer (Ramé-Hart Instrument Co., Succasunna, NJ). The as-received dry PVDF membrane was placed on a flat surface. A drop of ultrapure water was dispensed by a Gilmont<sup>®</sup> micrometer syringe (Cole-Parmer, Vernon Hills, IL) onto the membrane surface. The contact angle was measured through the liquid (i.e., water).

Membrane zeta potentials were measured with an Anton Paar (Ashland, VA) SurPASS electrokinetic analyzer. Each measurement required two 55 mm  $\times$  25 mm membrane samples, one of which was punched with two holes to allow flow into and out of the clamping cell. The two membrane samples were separated by two polypropylene spacers to form a flow channel. The clamping cell configuration was recommended by the manufacturer. The electrolyte solution flowed tangentially across the membrane surface in this configuration to avoid potential effects due to specific ion adsorption inside the porous structure of the membrane [17]. The applied pressure was 300 mBar. A



fresh  $10^{-3}$  M aqueous potassium chloride solution was used as the background electrolyte. The electrolyte solution pH was adjusted with a sodium hydroxide solution (0.1 M) to reach an initial pH greater than 10. The instrument adjusted the electrolyte solution pH by auto-titrating with a hydrochloric acid aqueous solution (0.1 M) and measured zeta potential values at pH values ranging from 10 to 3.

Pristine and fouled membranes were imaged with an FEI Quanta 650 scanning electron microscope (Hillsboro, OR). Samples were air-dried before imaging. The dried membrane was freeze-fractured to minimize distortion to the cross sectional area. None of the samples were sputter coated. Images were taken in a low vacuum environment (0.55 Torr) to prevent volatile oil, present on some of the fouled membranes, from damaging the instrument. The large field detector was utilized in low vacuum mode. The accelerating voltage was 10.0 kV.

### **2.3 Model fouling media formulations**

The four model fouling media included a suspension of latex beads and emulsions of soybean, motor and crude oil. Each oil emulsion had a total mass concentration (oil plus surfactant) of 200 ppm, and the latex bead suspension had a mass concentration of 200 ppm of latex beads. For each crossflow test, 8 L of feed mixture was prepared. An Oakton Con110 (Vernon Hills, IL) was used to measure emulsion conductivity. The fouling media turbidity was measured with a Hach 2100AN turbidity meter (Loveland, CO). Zeta potentials of model fouling media were measured using a Zetasizer Nano (Malvern, UK) at 25 °C using DTS-1070 cells.

As suggested by the manufacturer, the latex bead suspension container was carefully rolled on a flat surface and then immersed in a sonication bath briefly (30 seconds) to ensure a homogenous suspension. 16 g of 10 wt% latex bead suspension was

diluted to 200 ppm by adding ultrapure water (8 L). The ionic strength was adjusted to  $10^{-5}$  M using the ionic strength adjustment solution. 8 mL of pH=6 buffer was added to maintain the suspension pH at 6. Suspension concentration and pH were set to be consistent with earlier studies [10, 18].

The soybean oil emulsion was prepared with an oil-to-surfactant (Xiameter) mass ratio of 9:1. The oil and surfactant were mixed with ultrapure water (2 L) in a Waring<sup>®</sup> LBC15 laboratory blender (Torrington, CT) at 20,000 rpm for 3 minutes to achieve a concentrated mixture. To dilute the emulsion, 3 L of ultrapure water was first added to the feed tank, then the concentrated mixture was added, and then another 3 L of ultrapure water was added. The crude oil emulsion was prepared slightly different in that the oil-to-surfactant (Triton) mass ratio of 8:2, and the blending time was 5 minutes. The measured conductivity was approximately  $1.1 \mu\text{S}/\text{cm}$  and the measured pH was around 5.6, both of which corresponded to those of  $\text{CO}_2$ -equilibrated water [19]. Therefore, the salt concentrations of the crude oil emulsion can be considered negligible.

The motor oil emulsion had a salt concentration of 1 wt% to simulate the salt content in produced waters [20]. The motor oil concentrate mixture was prepared using an oil-to-surfactant (Triton) mass ratio of 8:2. Oil, surfactant, NaCl (20 g), 1 N NaOH solution (5 mL) and ultrapure water (2 L) were blended together for 5 minutes at 20,000 rpm. The salt was added in proportion to the volume to achieve a salt concentration of 1 wt% to minimize the potential effect of salt concentration change on emulsion stability [21]. Then, the final emulsion was mixed in the feed tank by first dissolving NaCl (60 g) in 3 L of ultrapure water, adding the concentrated mixture, and then adding another 3 L of ultrapure water. The final emulsion volume was 8 L, and had an organic concentration of 200 ppm, a salt concentration of 1 wt%, and a pH of 8-9.

## 2.4 Constant permeate flux crossflow fouling experiment

Fouling studies are often performed at constant TMP, while most industrial operations employ constant permeate flux processes [22]. Pretreated membranes were challenged with model fouling media in constant permeate flux crossflow fouling experiments. The apparatus is described in detail elsewhere [18]. A simplified diagram of the system is shown in Supporting Information Figure S - 2. The membrane sample surface area was 19 cm<sup>2</sup>. The feed crossflow velocity was 43 cm/s (feed flow rate = 2 L/min, Re = 2500). Future studies will report results at various feed flow rates. The feed pressure (i.e., membrane upstream pressure) was maintained at 30 psig (308 kPa) by a backpressure regulator. The permeate flow rate of each membrane cell was controlled by a peristaltic pump on each permeate line that operated in feedback-control mode with a Coriolis mass flow meter. Three membrane samples were tested simultaneously in all experiments. Transmembrane pressures were monitored throughout the experiment with differential pressure transducers and recorded using a LabVIEW<sup>®</sup> program. At the beginning of each experiment, the system was stabilized by circulating ultrapure water at the specified feed flow rate, feed pressure and permeate flow rate. Afterwards, the feed was switched to a model fouling medium.

Latex particle and oil droplet sizes and size distributions were measured inline with a Microflow<sup>™</sup> liquid particle analyzer (JM Canty, Inc., Buffalo, NY) during crossflow fouling tests. The liquid particle analyzer was installed upstream of the membrane cells. The particle analyzer consisted of an optical microscope and a high-speed camera. Videos of the feed solution during a fouling experiment were recorded and analyzed with the Canty Vision Client software. Latex particles and oil droplets were

identified by their circular geometry. The minimal droplet size that can be detected by this system was about 0.7  $\mu\text{m}$ .

The oil emulsion organic carbon concentration was measured using a total organic carbon analyzer  $V_{\text{CSH}}$  (Shimadzu, Japan). Organic rejection,  $R$ , was calculated based on the concentrations of feed and permeate samples:

$$R = \left( 1 - \frac{C_{\text{permeate}}}{C_{\text{feed}}} \right) \times 100\% \quad [2]$$

where  $C_{\text{feed}}$  and  $C_{\text{permeate}}$  are the feed and permeate concentrations, respectively. The organic concentration is based on turbidity for the latex bead suspension or total organic carbon concentration for oil emulsions.

## 2.5 Critical and threshold flux determination

To determine critical and threshold fluxes, flux stepping fouling experiments were performed using the constant flux crossflow apparatus [10, 12]. The permeate flux was increased stepwise every 15 minutes from lower fluxes to higher fluxes in an increment of 10  $\text{Lm}^{-2}\text{hr}^{-1}$  (LMH). Transmembrane pressures were continuously monitored during each interval. Figure 1 schematically illustrates critical and threshold flux determination.  $TMP_{\text{avg}}$  is the arithmetic mean of all TMP values recorded during one flux step. The  $TMP_{\text{avg}}$  value of each flux step is plotted versus flux. The solid blue line represents the TMP-flux relationship in the absence of fouling (i.e., pure water filtration).

The critical flux may take one of the two forms: the strong form critical flux,  $J_{\text{CS}}$ , if there is no adsorptive fouling, or the weak form critical flux,  $J_{\text{CW}}$ , if adsorptive fouling is observed. Adsorptive fouling is the spontaneous adsorption of foulant to a membrane surface, which is independent of permeate flux [18]. For a given filtration, only one critical flux can be observed, either the strong or the weak form, depending on

whether foulant adsorption affects the membrane mass transport resistance or not. In many cases, the critical flux is so low that it cannot be measured due to instrument limitations. Line A is the linear regression of  $TMP_{avg}$  as a function of flux below the critical flux. If foulant adsorption does not occur or does not affect the membrane transport resistance, Line A is identical to that for pure water filtration and intercepts the axes at the origin with a slope equals to the clean membrane resistance (cf., Figure 1). Line B is the linear regression of  $TMP_{avg}$  between the critical and threshold fluxes. Line C is the linear regression of the first two  $TMP_{avg}$  values that deviate from Line B. The intercepts of Lines A and B and Lines B and C are identified as the critical and threshold fluxes, respectively [18]. Variations in the flux-stepping technique can lead to differences in critical and threshold flux values [23, 24]. Nevertheless, a qualitative comparison can be drawn among separate measurements, as long as the experimental procedure and analysis technique are consistent.

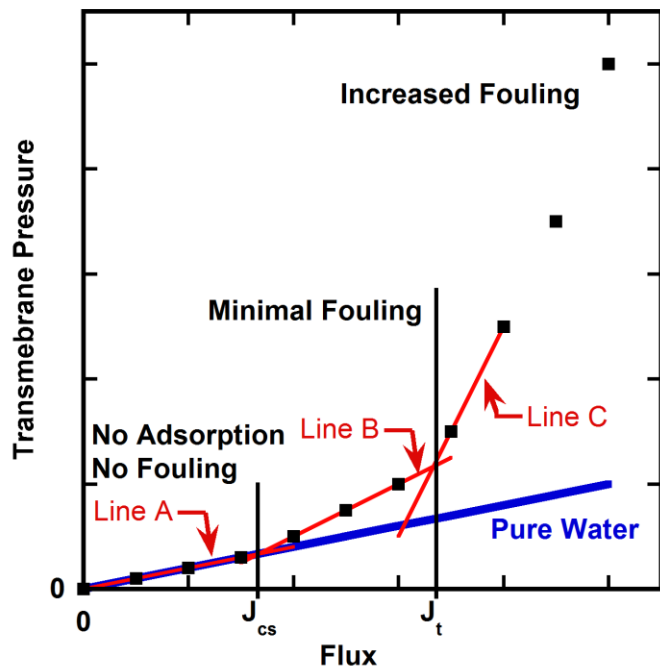


Figure 1. A hypothetical illustration of critical and threshold flux determination based on  $TMP_{avg}$  calculated from a flux-stepping experiment [12, 18]. Line A is the linear regression of  $TMP_{avg}$  below  $J_{CS}$ . Line B is the linear regression of  $TMP_{avg}$  between the critical and threshold fluxes. Line C is the linear regression of the first two  $TMP_{avg}$  values above the threshold flux. The solid blue line represents the TMP-flux relationship in the absence of fouling (i.e., pure water filtration). The intercepts of Lines A and B and Lines B and C are the critical and threshold fluxes, respectively.

### 3. RESULTS AND DISCUSSION

#### 3.1 Membrane characteristics

The PVDF membrane had a nominal pore rating of 0.2  $\mu\text{m}$ . According to the surface and cross-sectional area SEM images presented in Figure 2, the porous structure appeared symmetric, in agreement with the manufacturer's characterization of this

membrane. The PVDF membrane had a pure water permeance of 10,000 LMH/bar, which corresponds to a mass transfer resistance of 0.01 kPa/LMH.

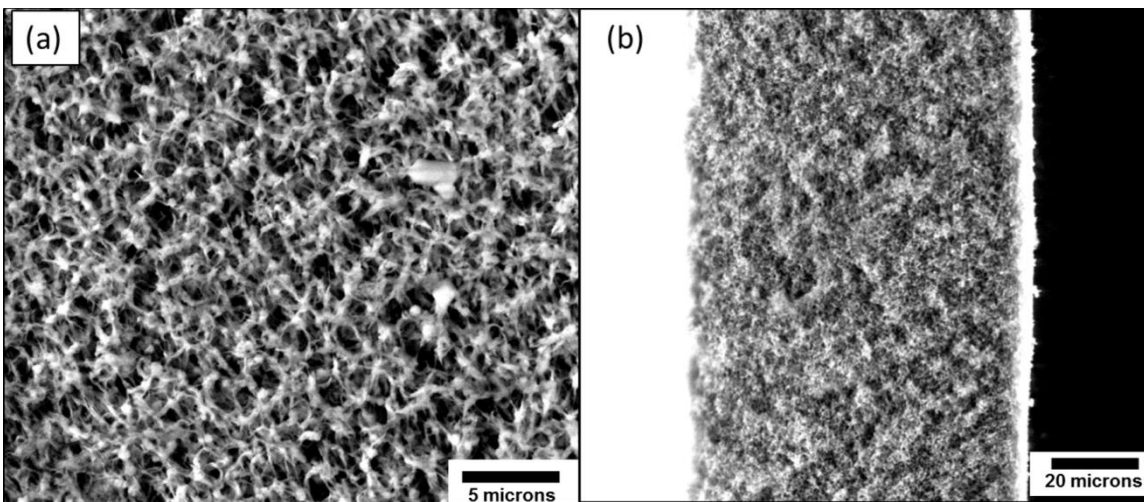


Figure 2. SEM images of PVDF MF membrane: (a) Surface, and (b) Cross-section.

The sessile drop contact angle with respect to water was  $139\pm 5^\circ$ , indicating that the PVDF membrane was hydrophobic. As shown in Figure 3, based on the zeta potential measurements, the surface of the PVDF membrane appeared to be negatively charged in the same pH range of the foulants (i.e., pH = 5.6-9). Although PVDF is electrically neutral in air, it appeared to have a negative surface charge when immersed in water. A similar phenomenon has been observed for many hydrophobic polymeric materials, and it has been attributed to the specific adsorption of hydroxide ions in the Stern layer [25-27]. The measured zeta potential value is not the true surface charge, rather the charge at the Stern layer, which is typically 3-5 Å from the polymer/water interface [28]. In this study, the terms “zeta potential” and “surface charge” are used interchangeably.

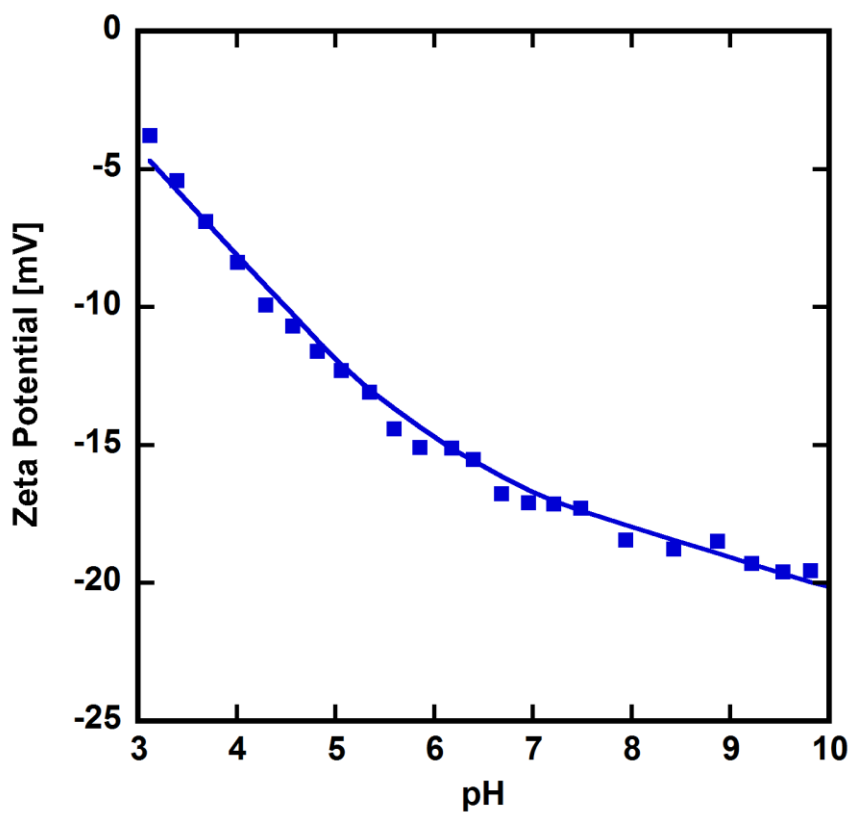


Figure 3. Zeta potential of the PVDF membrane in the pH range of 3-10. The background electrolyte was  $10^{-3}$  M KCl solution.

### 3.2 Fouling media characteristics

Latex beads and oil droplets were negatively charged. Latex beads had a zeta potential of  $-38.5 \pm 4.9$  mV. The measured zeta potential was more negative than that of pristine polystyrene (i.e., -29 mV), likely due to the presence of anionic surfactants added by the manufacturer to stabilize the latex beads [29, 30]. Soybean, motor and crude oil droplets had zeta potential values of  $-22.2 \pm 0.8$ ,  $-8.3 \pm 0.4$  and  $-20.0 \pm 1.3$  mV, respectively. The added salt content led to the relatively neutral zeta potential of motor oil emulsion. As stated earlier, the PVDF membrane had a negative charge in water.



Thus, the negative charges of the membrane and foulants should contribute to electrostatic repulsion between them [31, 32].

Droplet size distributions, as measured by the Canty Microflow™ system, were stable throughout fouling experiments. The four model fouling media had average particle/oil droplet sizes ranging from 3.4 to 4 μm. The average sizes are the arithmetic mean size of all particles detected by the Microflow™ inline particle analyzer during the course of a fouling experiment, while the feed was circulated at 2 L/min and 308 kPa. Figure 4 shows a snapshot of the size distributions of all droplets detected in the first 10 minutes of a fouling experiment based on the number of particles. A log-normal distribution was fit to the particle/oil droplet size distributions using the MATLAB® distribution fitting toolbox. Standard deviations,  $\sigma$ , of the fit were calculated and are reported in the figures. The latex bead suspension and the soybean oil emulsion had somewhat narrower distributions than those of the motor and crude oil emulsions. As shown in Figure 4, the latex bead suspension average particle size was larger than the nominal size of one bead (3.2 μm diameter as measured under optical microscope by the manufacturer), presumably due to some particle agglomeration. The motor oil emulsion showed a slightly larger average droplet size than that of the soybean or crude oil emulsions. Almost all of the droplets were less than 10 μm in diameter. The particle analyzer can only detect particles/oil droplets as small as 0.7 μm, so sub-micron size oil droplets and soluble organics, which cannot be measured, might exist in the oil emulsions. In general, our goal was to choose latex beads and oil/water emulsions with particles that were all roughly the same size and that were larger than the nominal average pore size of the membrane, so that the membrane would exhibit some rejection to the various foulants and so that effects other than foulant size (e.g., foulant surface

charge) could be explored. More foulant characteristics, including surface tension, turbidity and refractive index, are provided in the Supporting Information.

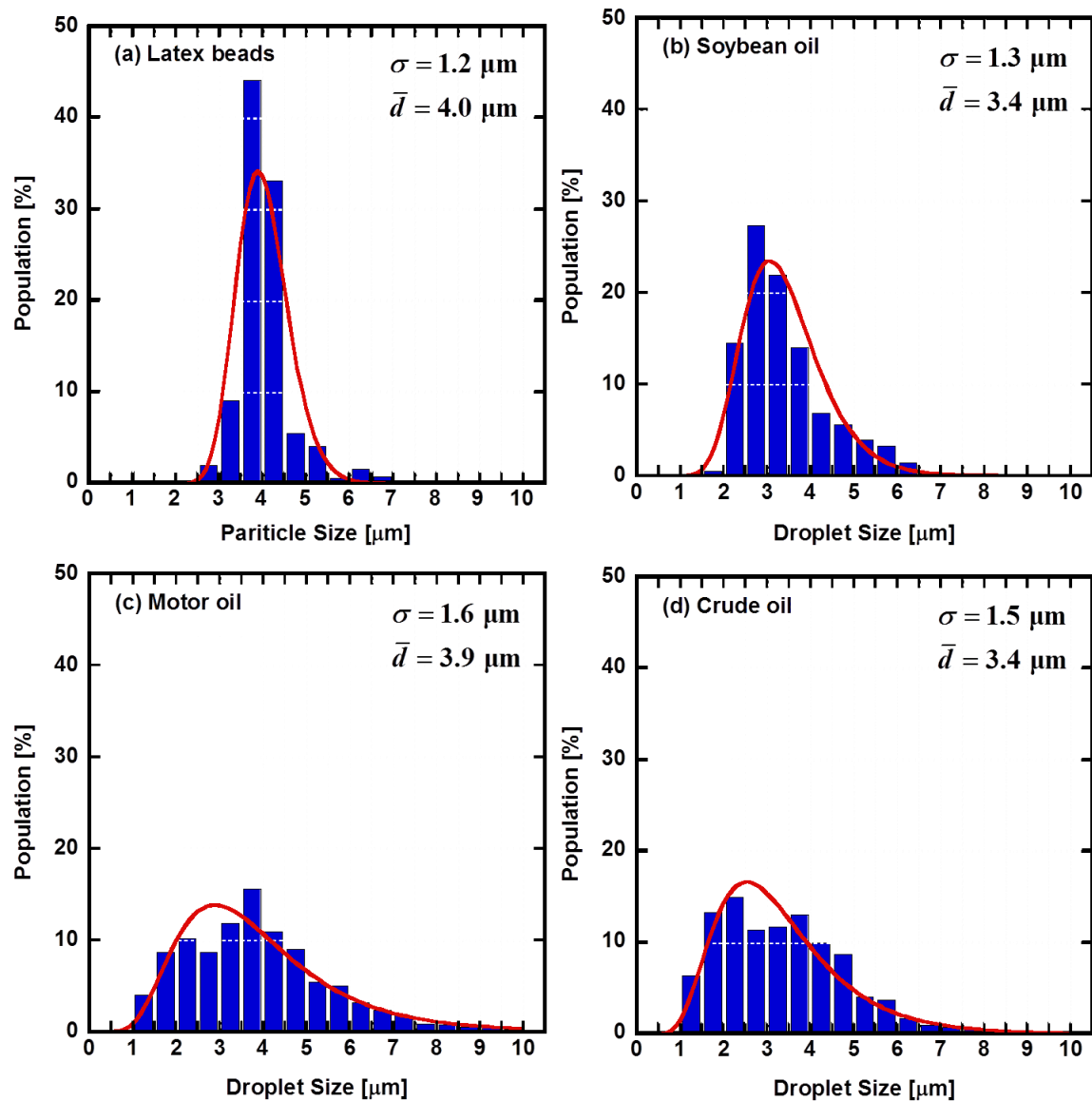


Figure 4. Latex bead suspension, and soybean, motor and crude oil emulsions particle and oil droplet size distributions determined by the Microflow™ particle analyzer. The population percentage was calculated based on the number of particles. The particle size distributions were based on droplets captured during the first 10 minutes of fouling experiments. These distributions did not vary throughout the experiments. The red lines are the log-normal fitting of particle/droplet size distributions, with a standard deviation of  $\sigma$ .

### 3.3 Critical and threshold flux

The concept of critical flux were originally proposed by Field *et al.* in 1995 [3]. Later, Field and Pearce clarified differences among critical, threshold, and sustainable flux [14]. The threshold flux,  $J_t$ , was developed with operational considerations in mind [14]. The threshold flux separates the slow fouling regime, where the rate of fouling is nearly constant with respect to permeate flux, from the rapid fouling regime, where the rate of fouling increases markedly with the amount of solution filtered (or, equivalently, time, in the case of a constant flux filtration) [14].

In our study, the critical and threshold fluxes were determined using the flux-stepping technique for each fouling medium under identical operating conditions. Figure 5 presents the TMP profiles and imposed flux steps as functions of time for each medium. In the crossflow membrane cell setup, the hydraulic pressure drop along the membrane cell flow path contributed to the TMP measured by differential pressure transducers. The hydraulic pressure drop exceeded the TMP at low fluxes, such as 20 and 30 LMH. Experimental uncertainties were also greatest at low fluxes due to the limitations of the differential pressure transducers. Therefore, the  $TMP_{avg}$  values for fluxes at 20 and 30 LMH were not included in the critical and threshold fluxes determinations. The  $TMP$  and  $TMP_{avg}$  values presented in this study were corrected by subtracting the hydraulic pressure drop from the measured pressure.

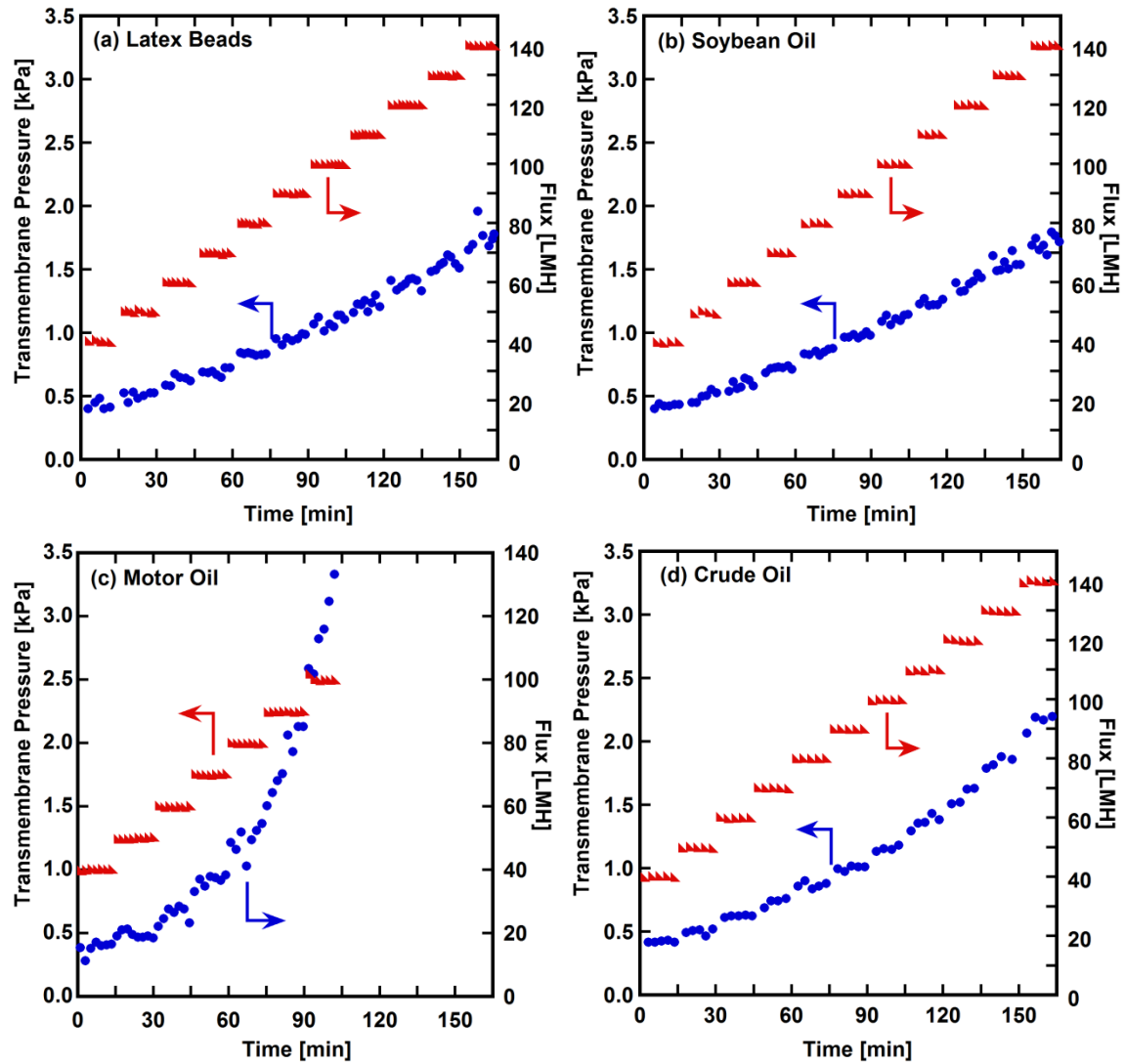


Figure 5. TMP profiles and the imposed flux steps as functions of time for (a) latex bead suspension and (b) soybean, (c) motor and (d) crude oil emulsions. The flux was increased step-wise every 15 minutes in 10 LMH intervals.

Figure 6 presents the  $TMP_{avg}$  of each flux interval with respect to flux. The solid blue line is the TMP-flux relationship based on the clean membrane resistance of 0.01 kPa/LMH. Critical and threshold fluxes were calculated based on the linear regression of

$TMP_{avg}$  at each flux step [18].  $TMP_{avg}$ -flux profiles for the latex bead suspension and for the soybean and crude oil emulsions followed the pure water filtration line at low fluxes, so the membrane resistance was equal to that of a clean membrane. Linear regressions intercepted the axes at the origin. Therefore, critical fluxes determined were the strong form critical flux, indicating no adsorptive fouling. Linear regressions of Line B (cf., Figure 6) showed larger slopes than that of pure water filtration.  $J_{CS}$  and  $J_t$  were determined for all fouling media, except for the motor oil emulsion. For the motor oil emulsion, the  $TMP_{avg}$  increased rapidly over the entire flux range studied, as shown in Figure 6(c). Critical and threshold fluxes for motor oil emulsion were likely to be lower than 50 LMH, although enough experimental data for a definitive linear regression could not be collected. This flux value can be validated against fouling results from constant permeate flux fouling experiments [33]. The TMP profile showed a continuous increase at 50 LMH, suggesting that 50 LMH was above the membrane threshold flux with the motor oil emulsion (cf., Figure 8(c)), so our interpretation of the flux-stepping experiment is consistent with the constant permeate flux results.

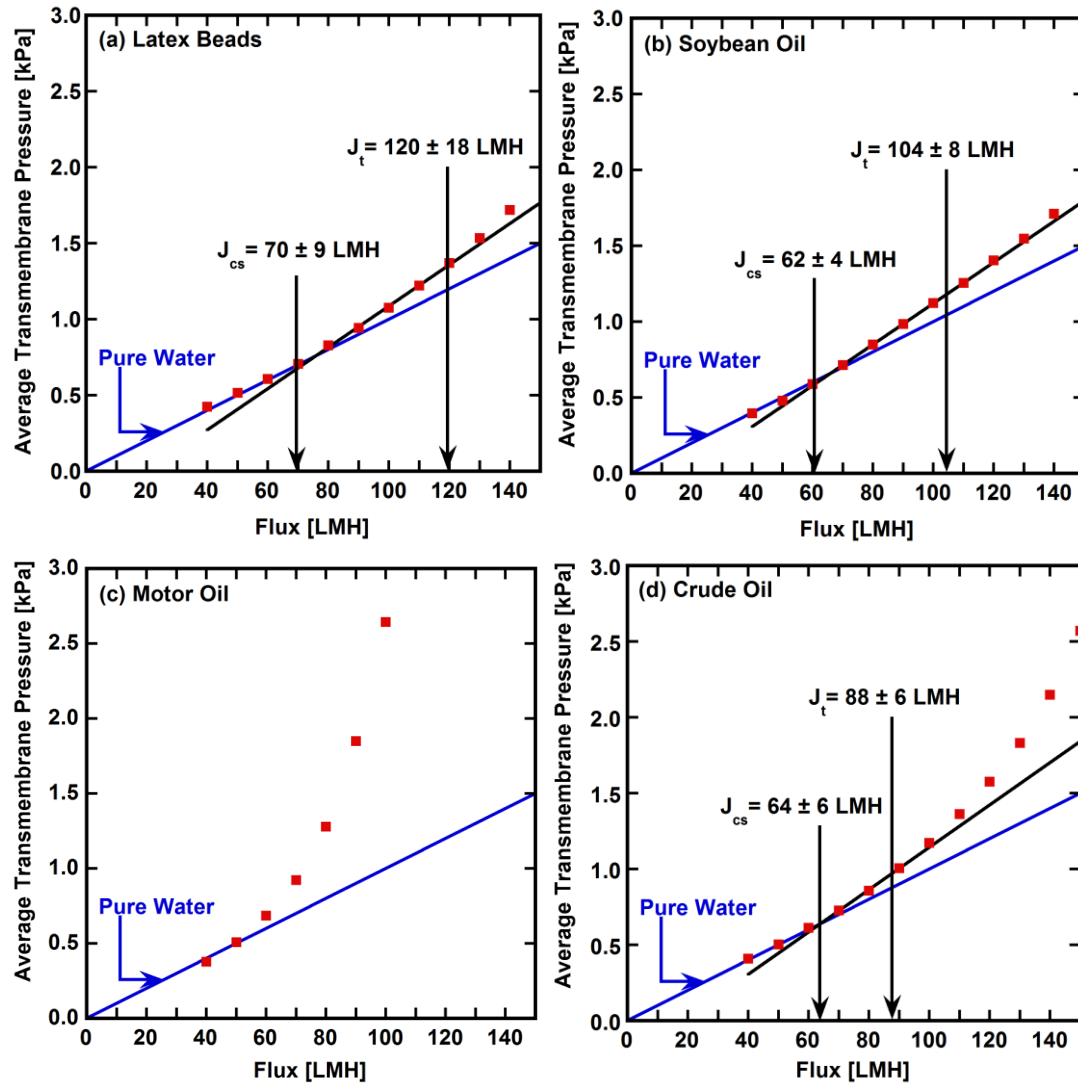


Figure 6.  $TMP_{avg}$  plotted as a function of flux. The solid blue lines are the TMP-flux relationship for pure water filtration. The strong form critical flux,  $J_{cs}$ , and the threshold flux,  $J_t$ , are shown for each model fouling medium, except for the motor oil emulsion.

Critical and threshold fluxes for each fouling medium are summarized in Table 1. The standard deviation was estimated based on results from three membrane samples that were tested simultaneously.

Table 1. Critical and threshold fluxes determined from flux-stepping experiments.

	Critical Flux [LMH]	Threshold Flux [LMH]
Latex Beads	70 ± 9	120 ± 18
Soybean Oil	62 ± 4	104 ± 8
Motor Oil	< 50	< 50
Crude Oil	64 ± 6	88 ± 6

### 3.3.1. Critical flux

Critical fluxes for the latex bead suspension and for the soybean and crude oil emulsions were statistically the same. Bacchin *et al.* proposed that the critical flux results from balanced foulant deposition and removal mechanisms. This balance can be formally expressed as follows: [34]

$$N = JC - D \frac{dC}{dy} + p(\zeta) + q(\tau) \quad [3]$$

where  $N$  is the net foulant deposition rate,  $J$  is the convective flux to the membrane surface,  $C$  is the foulant concentration,  $y$  is the distance from the membrane surface,  $D$  is the foulant Brownian diffusion coefficient,  $\zeta$  is the foulant zeta potential,  $p(\zeta)$  represents foulant deposition due mainly to membrane-foulant electrostatic interactions,  $\tau$  is shear stress at the membrane surface, and  $q(\tau)$  is the mass flux due to local hydrodynamic conditions. When a membrane process operates at steady state, and the



foulant net deposition rate is negligible,  $N$  approaches zero. For microfiltration of colloids and particles, Brownian diffusion is often negligible relative to the convective permeate flux. The magnitude of  $p(\zeta)$  is often smaller than that of  $q(\tau)$ , so the critical flux (or steady state flux) is: [34]

$$J_c \approx -\frac{q(\tau)}{C} \quad [4]$$

When membrane-foulant interactions are the most significant contributor to membrane fouling, the critical flux is more dependent upon  $p(\zeta)$ . Equation [4] represents the relative importance of relevant transport processes, so it should not be used for quantitative analysis [34].

In our study, membrane-foulant interactions were likely to vary depending on the fouling medium, whereas hydrodynamics,  $q(\tau)$ , and fouling media concentration,  $C$ , were kept consistent from one foulant to another. The consistency in critical fluxes, regardless of fouling medium, suggested that local hydrodynamics was the most significant factor governing critical flux. For the motor oil emulsion, a critical flux was not estimated, since strong membrane-foulant interactions apparently overwhelmed the influence of hydrodynamics, as suggested by the strong increase in  $TMP_{avg}$  with increasing flux. Motor oil droplets had a relatively low negative zeta potential relative to the other foulants, so it would have lower membrane-foulant and foulant-foulant electrostatic (EL) repulsion and stronger membrane-foulant attraction. Therefore, the critical flux of the motor oil emulsion may be more dependent on  $p(\zeta)$  than on  $q(\tau)$ .

### 3.3.2. Threshold flux

The threshold flux, which has been used interchangeably with the critical flux until recently, was investigated in many laboratory studies [14]. Field reported that “the

rate of fouling is the key” to determining the threshold flux and that “the fouling propensity depends on characteristics of the feed and the membrane, and the interaction between them” [14]. To study membrane-foulant interactions, Brant and Childress considered the three components of the extended Derjaguin-Landau-Verwey-Overbeek model: van der Waals, electrostatic double layer interactions, and acid-base interactions, and they reported that “the behavior of the membrane-colloid system is generally controlled by the colloid surface energetics” [31]. The initial foulant deposition is due to membrane-foulant interactions. The subsequent fouling is governed by EL interactions between the incoming foulant with deposited foulant after the membrane surface is covered by foulant [31].

In our study, the membrane and the hydrodynamic environment at the membrane surface were the same in all experiments (i.e., all foulants were tested at the same crossflow and permeate flow rates), so differences in fouling propensity among the different foulants were likely related to membrane-foulant and foulant-foulant EL interactions [31]. EL interactions are directly related to the zeta potential (surface charge) of the foulant [31]. The higher the foulant zeta potential, the stronger the electrostatic repulsion and the slower the rate of fouling [31]. The added salt in motor oil emulsion led to a low zeta potential and screened the electrostatic interactions [35]. In our experiments, a lower threshold flux was interpreted to represent a higher fouling propensity. Based on threshold fluxes calculated, the fouling propensity is as follows: latex beads < soybean oil < crude oil < motor oil.

For a given membrane, many factors, such as membrane and foulant surface charge, surface tension, surface rheology, and hydrophobicity, may contribute to fouling of the membrane [36]. We found it interesting that the threshold flux exhibited an

apparent correlation (cf., Figure 7) with foulant zeta potential. A similar influence of foulant zeta potential on fouling has been observed in ultrafiltration and microfiltration processes [37-39]. The effect of foulant zeta potential on membrane fouling was exacerbated by increasing salt concentration [37-39]. A more in-depth analysis of the forces between the foulants and this membrane will be reported separately, which we hope will further clarify the fundamental origins of fouling in these cases.

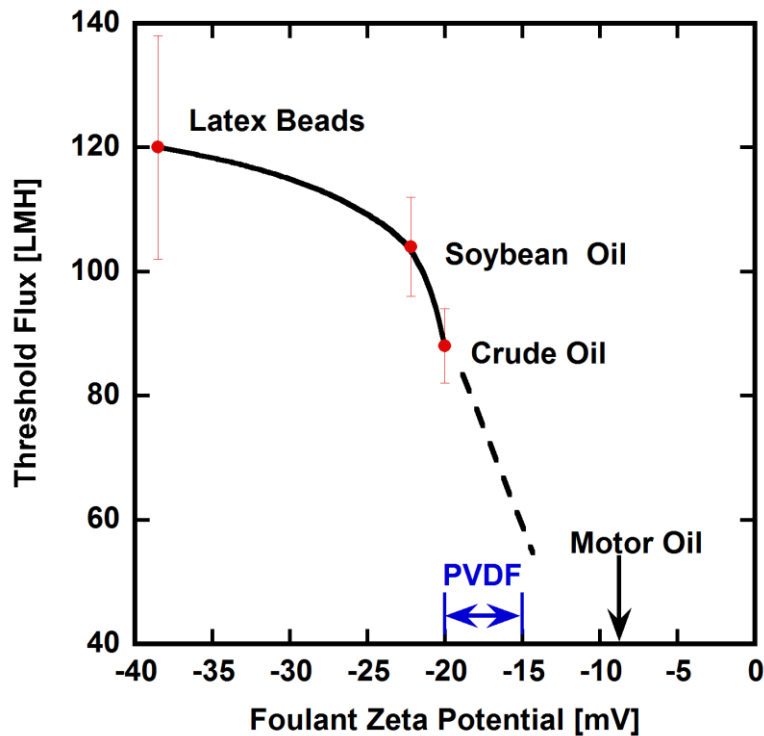


Figure 7. The threshold flux of each model fouling medium was plotted as a function of foulant zeta potential. The higher the zeta potential, the stronger the electrostatic repulsion and the higher the threshold flux. The line is drawn to guide the eye. The zeta potential of the PVDF membrane in the relevant pH range (pH = 5.6 to 9) is noted on the graph for reference.

### **3.4 Constant permeate flux crossflow fouling tests**

Constant permeate flux crossflow fouling experiments were performed with each fouling medium at two fluxes (50 and 150 LMH). Results are shown in Figure 8. For the latex bead suspension and the soybean and crude oil emulsions, 50 LMH was below their critical fluxes, and 150 LMH was above their threshold fluxes. However, 50 LMH and 150 LMH were above both the critical and threshold fluxes for the motor oil emulsion.

At 50 LMH, the TMP remained constant for the latex bead suspension and for the soybean and crude oil emulsions, indicating that no fouling occurred below their critical fluxes. For the motor oil emulsion, a steady increase in TMP was observed at a flux of 50 LMH. At 150 LMH, which was above the latex bead suspension threshold flux (i.e., 120 LMH), the TMP increased slightly initially and then approached a plateau. The TMP continuously increased throughout the experiments with all oil emulsions. The TMP increase was greater with oil emulsions than with latex beads. The extent of TMP increase reflected the fouling propensity and followed the order: latex beads < soybean oil < crude oil < motor oil. The order of fouling propensities based on TMP increase coincides with that determined by threshold fluxes (i.e., foulants that had lower threshold fluxes caused greater increases in TMP).

Latex beads are non-deformable rigid spheres that are significantly larger than the membrane pores. Therefore, latex beads could not permeate through the membrane porous structure. The oil organic rejections, as shown in Figure 8, were in the range of 50-80%. The organic rejection varied among different oils, but showed little variance at different fluxes, suggesting that the organic rejection was foulant-specific. The oil droplets, unlike latex beads, can deform and coalesce on the membrane surface. The transmembrane pressure may be able to overcome the capillary pressure of the oil, so oil

droplets larger than the membrane pores can partially enter the pores. The advancing portion of such an oil droplet may breakup with the lagging portion due to shear at the membrane surface [40-42]. This phenomenon can allow portions of larger droplets to pass through the membrane. Droplets smaller than the membrane pores and the soluble surfactants, which cannot be detected by the inline particle analyzer, may be transported through the membrane by the convective permeate flow. These combined effects would act to lower the organic rejection.

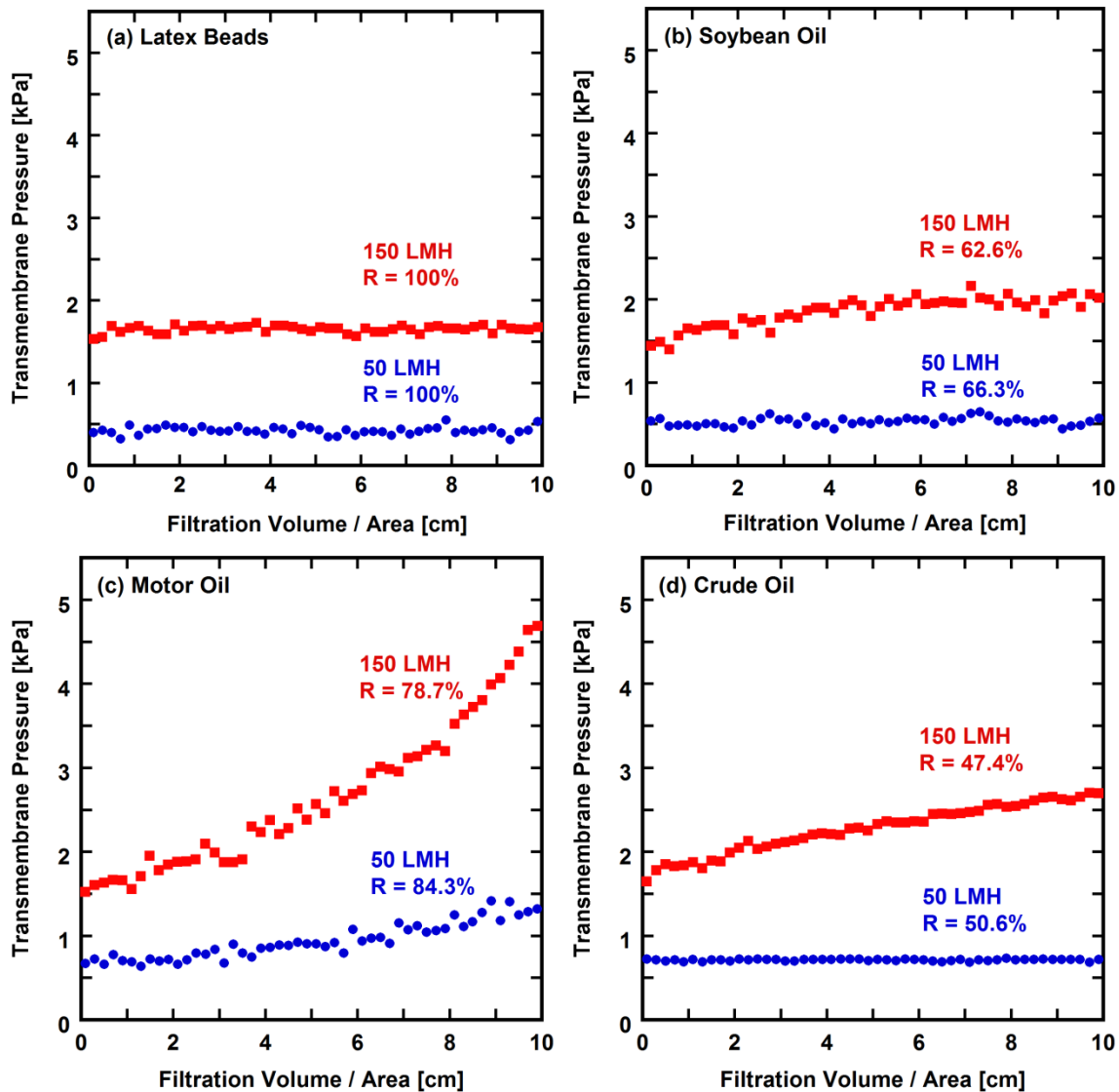


Figure 8. Transmembrane pressure profiles of constant permeate flux crossflow fouling tests with each model fouling medium at fluxes of 50 and 150 LMH. Feed flow rate = 2 L/min, crossflow velocity = 43 cm/s,  $Re = 2500$ , feed pressure = 30 psig (308 kPa), temperature = 25 °C. R is organic rejection.

Figure 9 and Figure 10 are SEM images of the feed and permeate faces of membranes fouled at 150 LMH in constant permeate flux fouling experiments. The latex beads are rigid spheres that are larger than membrane pore size, so the PVDF membrane

was able to reject 100% of them at both 50 and 150 LMH. As shown in Figure 9(a) and Figure 10(a), latex beads were rejected and attached to the feed side of the membrane, but no latex beads were observed on the permeate side of the membrane. Compared with the pristine membrane (cf., Figure 2), the motor oil-fouled membranes were covered by an oil layer, and the soybean and crude oil were able to plug a significant portion of the porous structure. The hydrophobic effect may contribute to foulant-foulant interactions due to the hydrophobic nature of the oil [35]. The deposited oil was more likely to attract incoming oil droplets and coalesce to form a cake layer than a pristine membrane surface. For all three oil emulsions, oil coverage was observed on both sides of membranes suggesting that oil was able to transport through the membranes, so organic rejections were less than 100%.

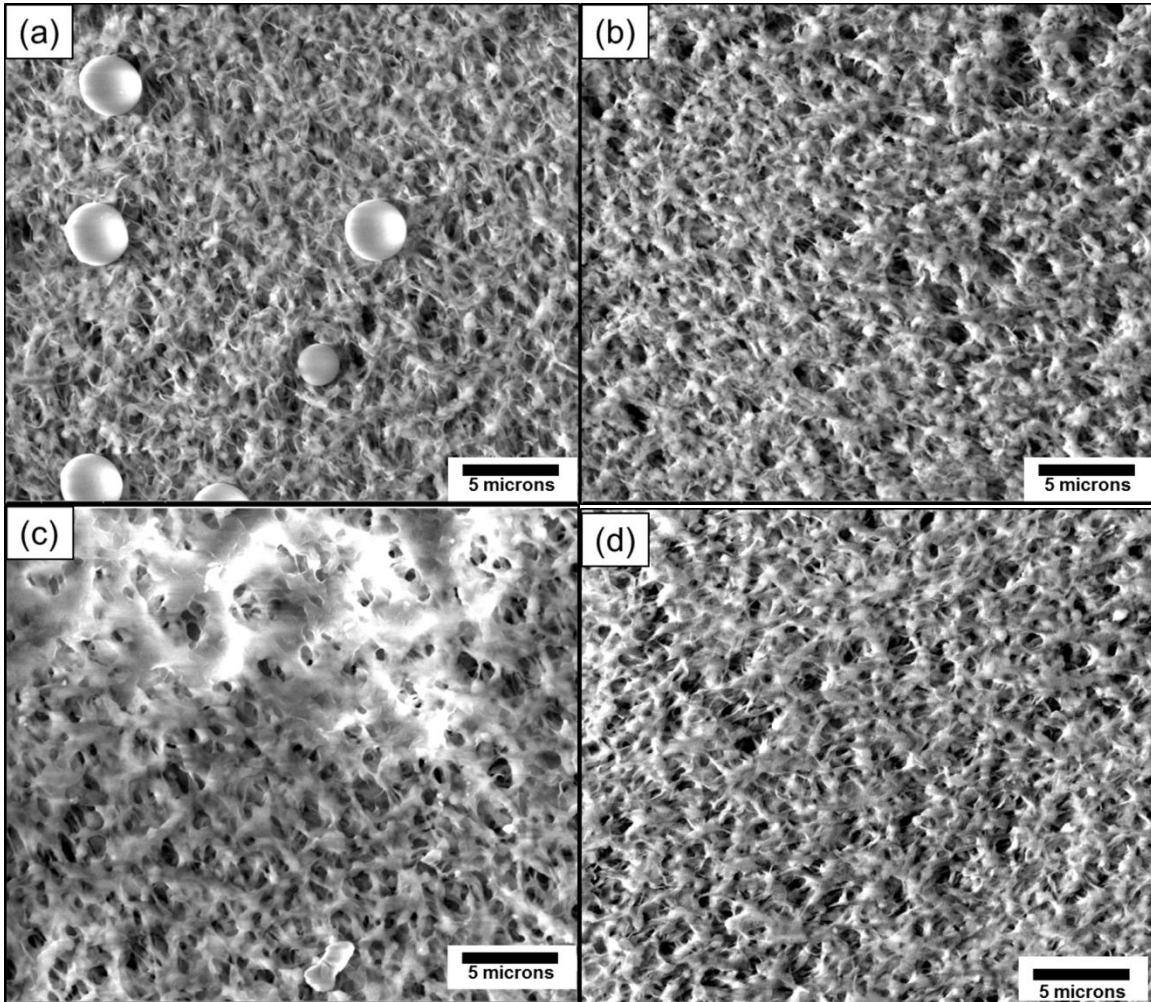


Figure 9. SEM images of the feed side of membranes fouled at 150 LMH flux during constant permeate flux crossflow fouling tests with: (a) latex bead suspension and (b) soybean, (c) motor and (d) crude oil emulsions.



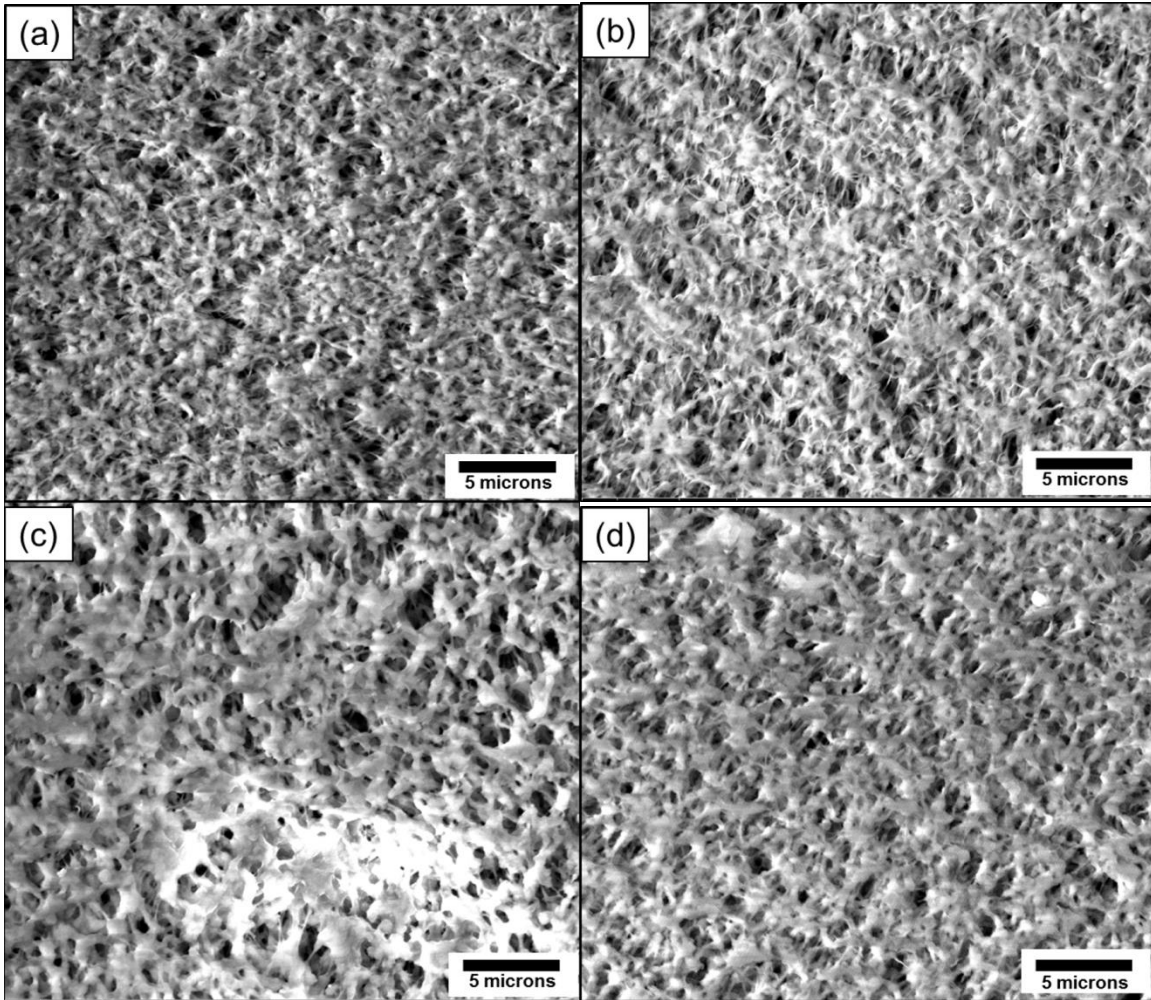


Figure 10. SEM images of the permeate side of membranes fouled at 150 LMH flux during constant permeate flux crossflow fouling tests with: (a) latex bead suspension and (b) soybean, (c) motor and (d) crude oil emulsions.

### 3.5 TMP jump

As shown in Figure 11, when membranes were challenged with motor and crude oil emulsions for an extended period of time, a three-stage TMP profile was observed. Following the initial steady increase in TMP discussed earlier, a sudden upturn or so-called “TMP jump” was observed, and then a pseudo-steady state TMP was reached. During a constant permeate flux fouling test, foulants are continuously brought to the

membrane surface at a constant rate by the convective flux. When the membrane surface and pores become partially or completely blocked by foulants, the local flux through the remaining open pores must increase to maintain the imposed overall constant permeate flux, so the foulant deposition rate at the remaining open pores must also increase [12, 43, 44]. The sudden TMP jump is often attributed to inhomogeneous fouling, as well as the high local flux during constant permeate flux operation [45]. Such TMP jumps indicate the onset of cake formation [12]. As shown in Figure 9 and Figure 10, oil coverage was found on both feed and permeate faces of the membrane, suggesting that oil deposited both inside the porous structure and on the membrane surface. Membranes experienced the TMP jump sooner with the motor oil emulsion than with the crude oil emulsion, in accordance with their fouling propensities.

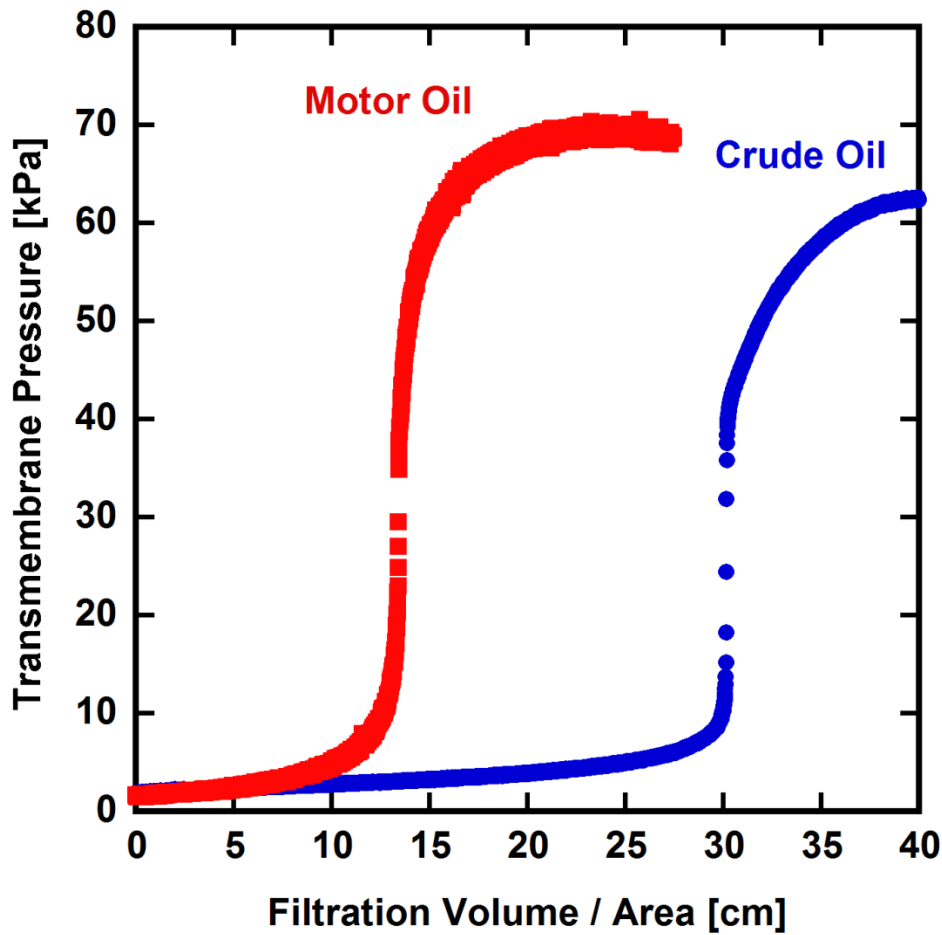


Figure 11. TMP profiles with motor and crude oil emulsion fouling at extended time. Feed flow rate = 2 L/min, crossflow velocity = 43 cm/s,  $Re = 2500$ , permeate flux = 150 LMH, feed pressure = 30 psig (308 kPa), temperature = 25 °C.

A similar phenomenon was observed by Liu *et al.* in a constant permeate flux microfiltration test using PVDF hollow fiber membranes with raw water containing kaolinite particles [46]. Liu separated fouling into three regimes: the initial slow fouling regime wherein membrane pore blocking takes place, a TMP jump regime indicating the cake layer formation, a final steady state regime with a stabilized cake layer [46]. In a recent report, Zydney and Ho simulated TMP profiles for cake filtration. The non-

compressible cake filtration presented a steady state TMP after the TMP jump, whereas the TMP could continue a linear increase with a highly compressible cake [44]. TMP jumps are commonly observed in membrane bioreactor (MBR) operations, which are also operated at constant permeate flux [45, 47, 48]. In some MBR operations, two TMP jumps may be observed: one TMP increase in the beginning of operation, then another TMP jump following an extended period of slow fouling [47]. The latter often “lead(s) to inoperability of the membranes”, according to Hwang *et al.* [47]. Membrane cleaning procedures are often instituted as soon as the TMP evolves into the upturn regime. As a result, the TMP is not always allowed to continuously rise beyond a pre-determined threshold value.

In this study, the TMP jump was allowed to fully develop. The TMP, instead of continuously increasing to beyond the system pressure limit (i.e., 308 kPa), gradually reached a pseudo-steady state. Traditionally, membrane processes are operated below the threshold flux to allow for slow fouling to reduce the cleaning frequency and lower operating cost. However, from an engineering point of view, the final pseudo-steady cake filtration regime may provide another operating window. Operating in the cake filtration regime may have potential benefits. The permeate flux would no longer be bounded by the threshold flux of the native membrane, so permeate throughput might be maximized. In the case of the motor oil emulsion, a permeate flux of 150 LMH was more than 3 times greater than its threshold flux, and it is almost two times higher for the crude oil emulsion. With higher throughput per membrane surface area, the number of membrane modules required and capital cost might be reduced significantly for a specified capacity. Further studies may focus on introducing the TMP jump sooner so that the filtration system can rapidly enter a pseudo-steady state operation, if the energy consumption can

be justified by the higher throughput. Both motor and crude oil emulsions displayed the TMP jump phenomenon and steady state cake filtration. Similar TMP profiles were not observed for the latex bead suspension or the soybean oil emulsion, but may be possible if experiment durations were extended.

#### **4. CONCLUSIONS**

Fouling of PVDF MF membranes was studied with a series of model fouling media: a latex bead suspension and soybean, motor and crude oil emulsions. Strong form critical fluxes and threshold fluxes were determined using the flux-stepping technique. Constant permeate flux crossflow fouling experiments were performed at two fluxes, one below the measured critical flux and the other above the measured threshold flux. Qualitatively, fouling propensity can be estimated based on either threshold flux or the extent of TMP increase at constant permeate flux operation. Given the same membrane and hydrodynamic conditions, the fouling propensity depended on the membrane-foulant and foulant-foulant interactions. Interestingly, based on these metrics, the tendency of these foulants to foul the membrane was greater in emulsions with lower zeta potentials, which might reduce electrostatic repulsion between the negative charges of the membrane surface and the foulants [31]. A three-stage TMP profile was observed with motor and crude oil emulsions at extended filtration times. The TMP jump indicated severe inhomogeneous fouling and the onset of cake formation. A pseudo-steady state cake filtration regime was recognized as a potential operating regime.

#### **5. ACKNOWLEDGEMENTS**

The authors gratefully acknowledge financial support from Pall Corporation, the National Science Foundation (NSF) Center for Layered Polymeric Systems (DMR-

0423914), and NSF Grant CBET 1160069. This study was also partially supported by the International Institute for Carbon Neutral Energy Research (WPI-I<sup>2</sup>CNER), sponsored by the Japanese Ministry of Education, Culture, Sports, Science and Technology.

## 6. REFERENCES

[1] C.E. Clark, J.A. Veil, Produced water volumes and management practices in the United States. Argonne National Laboratory, 2009, Report No: ANL/EVS/R-09-1.

<http://www.osti.gov/scitech/biblio/1007397>

[2] P. Boschee, Produced and flowback water recycling and reuse. *Oil and Gas Facilities*, 1 (2014) 16-21.

[3] R.W. Field, D. Wu, J.A. Howell, B.B. Gupta, Critical flux concept for microfiltration fouling. *Journal of Membrane Science*, 100 (1995) 259-272.

[4] R.W. Baker, *Membrane technology and applications*. 2<sup>nd</sup> ed., West Sussex, England: John Wiley & Sons, (2004).

[5] G.M. Geise, H.-S. Lee, D.J. Miller, B.D. Freeman, J.E. McGrath, D.R. Paul, Water purification by membranes: The role of polymer science. *Journal of Polymer Science Part B: Polymer Physics*, 48 (2010) 1685-1718.

[6] K. Parameshwaran, A.G. Fane, B.D. Cho, K.J. Kim, Analysis of microfiltration performance with constant flux processing of secondary effluent. *Water Research*, 35 (2001) 4349-4358.

[7] D.J. Miller, X. Huang, H. Li, S. Kasemset, A. Lee, D. Agnihotri, T. Hayes, D.R. Paul, B.D. Freeman, Fouling-resistant membranes for the treatment of flowback water from hydraulic shale fracturing: A pilot study. *Journal of Membrane Science*, 437 (2013) 265-275.

[8] J.R. Pressdee, S. Veerapaneni, H.L. Shorney-Darby, J.A. Clement, J.P. Van der Hoek, *Integration of membrane filtration into water treatment systems*. Denver: American Water Works Association Research Foundation and U.S. Department of the Interior, Bureau of Reclamation, (2006).

[9] L. Henthorne, Evaluation of membrane pretreatment for seawater reverse osmosis desalination. U.S. Department of the Interior, Bureau of Reclamation, 2007, Report No. 01-FC-81-0735.

<https://www.usbr.gov/research/AWT/reportpdfs/Report106.pdf>

[10] D.Y. Kwon, S. Vigneswaran, A.G. Fane, R.B. Aim, Experimental determination of critical flux in cross-flow microfiltration. *Separation and Purification Technology*, 19 (2000) 169-181.

- [11] C.H. Koo, A.W. Mohammad, F. Suja, M.Z. Meor Talib, Setting-up of modified fouling index (MFI) and crossflow sampler-modified fouling index (CFS-MFI) measurement devices for NF/RO fouling. *Journal of Membrane Science*, 435 (2013) 165-175.
- [12] D.J. Miller, S. Kasemset, D.R. Paul, B.D. Freeman, Comparison of membrane fouling at constant flux and constant transmembrane pressure conditions. *Journal of Membrane Science*, 454 (2014) 505-515.
- [13] D.J. Miller, P.A. Araújo, P.B. Correia, M.M. Ramsey, J.C. Kruithof, M.C.M. van Loosdrecht, B.D. Freeman, D.R. Paul, M. Whiteley, J.S. Vrouwenvelder, Short-term adhesion and long-term biofouling testing of polydopamine and poly(ethylene glycol) surface modifications of membranes and feed spacers for biofouling control. *Water Research*, 46 (2012) 3737-3753.
- [14] R.W. Field, G.K. Pearce, Critical, sustainable and threshold fluxes for membrane filtration with water industry applications. *Advances in Colloid and Interface Science*, 164 (2011) 38-44.
- [15] K.J. Howe, M.M. Clark, Fouling of microfiltration and ultrafiltration membranes by natural waters. *Environmental Science & Technology*, 36 (2002) 3571-3576.
- [16] Pall Corporation, Polyvinylidene fluoride (PVDF) membrane (hydrophobic).  
[http://www.pall.com/main/oem-materials-and-devices/product\\_page?id=47593](http://www.pall.com/main/oem-materials-and-devices/product_page?id=47593)
- [17] P. Fievet, A. Szymczyk, C. Labbez, B. Aoubiza, C. Simon, A. Foissy, J. Pagetti, Determining the zeta potential of porous membranes using electrolyte conductivity inside pores. *Journal of Colloid and Interface Science*, 235 (2001) 383-390.
- [18] D.J. Miller, D.R. Paul, B.D. Freeman, A crossflow filtration system for constant permeate flux membrane fouling characterization. *Review of Scientific Instruments*, 84 (2013) 035003-035011.
- [19] T.S. Light, E.A. Kingman, A.C. Bevilacqua, Conductivity of low concentrations of CO<sub>2</sub> dissolved in ultrapure water from 0-100 °C. in: *The 209th American Chemical Society National Meeting*, Anaheim, CA, 1995.
- [20] M.S. Blondes, K.D. Gans, J.J. Thordsen, M.E. Reidy, B. Thomas, M.A. Engle, Y.K. Kharaka, E.L. Rowan, National produced waters geochemical database v2.1 (provisional). U.S. Geological Survey, 2014.  
<http://energy.usgs.gov/EnvironmentalAspects/EnvironmentalAspectsofEnergyProductionandUse/ProducedWaters.aspx#3822349-data>
- [21] B.P. Binks, R. Murakami, S.P. Armes, S. Fujii, Effects of pH and salt concentration on oil-in-water emulsions stabilized solely by nanocomposite microgel particles. *Langmuir*, 22 (2006) 2050-2057.

- [22] R. Field, Fundamentals of fouling. In: K.-V. Peinemann, S.P. Nunes (Eds.) Membrane technology: Membranes for water treatment. Wiley-VCH, Weinheim, 2010, pp. 1-24.
- [23] J. Luo, S.T. Morthensen, A.S. Meyer, M. Pinelo, Filtration behavior of casein glycomacropeptide (CGMP) in an enzymatic membrane reactor: fouling control by membrane selection and threshold flux operation. *Journal of Membrane Science*, 469 (2014) 127-139.
- [24] J. Luo, L. Ding, Y. Wan, M.Y. Jaffrin, Threshold flux for shear-enhanced nanofiltration: Experimental observation in dairy wastewater treatment. *Journal of Membrane Science*, 409–410 (2012) 276–284.
- [25] D.O. Jordan, A.J. Taylor, The electrophoretic mobilities of hydrocarbon droplets in water and dilute solutions of ethyl alcohol. *Transactions of the Faraday Society*, 48 (1952) 346-355.
- [26] M. Elimelech, W.H. Chen, J.J. Waypa, Measuring the zeta (electrokinetic) potential of reverse osmosis membranes by a streaming potential analyzer. *Desalination*, 95 (1994) 269-286.
- [27] J.K. Beattie, The intrinsic charge on hydrophobic microfluidic substrates. *Lab on a Chip*, 6 (2006) 1409-1411.
- [28] R.F. Probstein, *Physicochemical Hydrodynamics: An Introduction*. 2nd ed., New York: John Wiley & Sons, (1994).
- [29] A. Bismarck, M.E. Kumru, J. Springer, Characterization of Several Polymer Surfaces by Streaming Potential and Wetting Measurements: Some Reflections on Acid–Base Interactions. *Journal of Colloid and Interface Science*, 217 (1999) 377-387.
- [30] B.J. Kirby, E.F. Hasselbrink, Zeta potential of microfluidic substrates: 2. Data for polymers. *ELECTROPHORESIS*, 25 (2004) 203-213.
- [31] J.A. Brant, A.E. Childress, Assessing short-range membrane–colloid interactions using surface energetics. *Journal of Membrane Science*, 203 (2002) 257-273.
- [32] A.E. Childress, M. Elimelech, Effect of solution chemistry on the surface charge of polymeric reverse osmosis and nanofiltration membranes. *Journal of Membrane Science*, 119 (1996) 253-268.
- [33] S.P. Beier, G. Jonsson, Critical flux determination by flux-stepping. *AIChE Journal*, 56 (2010) 1739-1747.
- [34] P. Bacchin, P. Aimar, R.W. Field, Critical and sustainable fluxes: Theory, experiments and applications. *Journal of Membrane Science*, 281 (2006) 42-69.
- [35] C.J. van Oss, *Interfacial Forces in Aqueous Media*. 2<sup>nd</sup> ed., Boca Raton, FL: CRC Press, (2006).



- [36] M. Cheryan, *Ultrafiltration and Microfiltration Handbook*. 2nd ed., Lancaster, PA: CRC Press, (1998).
- [37] S. Li, S.G.J. Heijman, J.Q.J.C. Verberk, J.C. van Dijk, Influence of Ca and Na ions in backwash water on ultrafiltration fouling control. *Desalination*, 250 (2010) 861-864.
- [38] G. Singh, L. Song, Quantifying the effect of ionic strength on colloidal fouling potential in membrane filtration. *Journal of Colloid and Interface Science*, 284 (2005) 630-638.
- [39] S. Vigneswaran, D.-Y. Kwon, Effect of ionic strength and permeate flux on membrane fouling: Analysis of forces acting on particle deposit and cake formation. *KSCE Journal of Civil Engineering*, (2014) 1-8.
- [40] T. Darvishzadeh, N.V. Priezjev, Effects of crossflow velocity and transmembrane pressure on microfiltration of oil-in-water emulsions. *Journal of Membrane Science*, 423–424 (2012) 468-476.
- [41] P. Kajitvchyanukul, Y.-T. Hung, L.K. Wang, Oil water separation. In: L.K. Wang, Y.-T. Hung, N.K. Shammas (Eds.) *Advanced Physicochemical Treatment Processes*. Humana Press Inc., Totowa, NJ, 2007.
- [42] E.N. Tummons, V.V. Tarabara, J.W. Chew, A.G. Fane, Behavior of oil droplets at the membrane surface during crossflow microfiltration of oil-water emulsions. *Journal of Membrane Science*, 500 (2016) 211-224.
- [43] D.J. Miller, S. Kasemset, L. Wang, D.R. Paul, B.D. Freeman, Constant flux crossflow filtration evaluation of surface-modified fouling-resistant membranes. *Journal of Membrane Science*, 452 (2014) 171-183.
- [44] C.-C. Ho, A.L. Zydney, Transmembrane pressure profiles during constant flux microfiltration of bovine serum albumin. *Journal of Membrane Science*, 209 (2002) 363-377.
- [45] A.G. Fane, Sustainability and membrane processing of wastewater for reuse. *Desalination*, 202 (2007) 53-58.
- [46] Q.-F. Liu, S.-H. Kim, Evaluation of membrane fouling models based on bench-scale experiments: A comparison between constant flowrate blocking laws and artificial neural network (ANNS) model. *Journal of Membrane Science*, 310 (2008) 393-401.
- [47] B.-K. Hwang, C.-H. Lee, I.-S. Chang, A. Drews, R. Field, Membrane bioreactor: TMP rise and characterization of bio-cake structure using CLSM-image analysis. *Journal of Membrane Science*, 419–420 (2012) 33-41.
- [48] Y. Ye, V. Chen, A.G. Fane, Modeling long-term subcritical filtration of model EPS solutions. *Desalination*, 191 (2006) 318-327.

SUPPORTING INFORMATION FOR

**Fouling propensity of a poly(vinylidene) fluoride microfiltration membrane to several model oil/water emulsions**

**Zhengwang He, Daniel J. Miller<sup>1</sup>, Sirirat Kasemset<sup>2</sup>, Lu Wang, Donald R. Paul, Benny D. Freeman\***

Department of Chemical Engineering, Center for Energy and Environmental Resources, and Texas Materials Institute, The University of Texas at Austin, 10100 Burnet Road Building 133, Austin, TX 78758

\*Corresponding author (Tel: +1-512-232-2803; Email: [freeman@che.utexas.edu](mailto:freeman@che.utexas.edu))

1. Current address: Joint Center for Artificial Photosynthesis, Lawrence Berkeley National Laboratory, 1 Cyclotron Road, Berkeley CA 94702
2. Current address: Evonik Corporation, 4201 Evonik Road, Theodore, AL 36582

Submission to the *Journal of Membrane Science*

## 1. SURFACTANTS CHEMICAL STRUCTURE

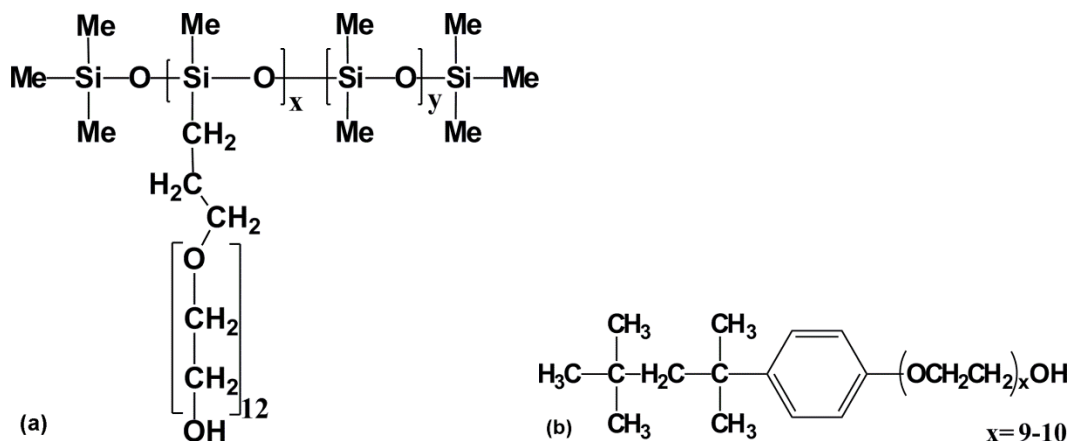


Figure S - 1. Chemical structures of non-ionic surfactants: (a) Xiameter® OFX-193, and (b) Triton™ X-100. Xiameter and Triton have, on average, 12 and 9.5 ethylene oxide (EO) units per molecule, respectively.

## 2. FOULANT CHARACTERISTICS

The turbidity of fouling media was measured with a Hach 2100AN turbidity meter (Loveland, CO). The refractive index of various oils was measured with an Abbe type refractometer (Fisher Scientific, Fairlawn, NJ) at 24 °C. The uncertainty of the refractive index measurement was  $\pm 0.0002$ . The pendant drop method was used to measure surface tensions of fouling media. Surface tensions were calculated by the DROPimage software (Ramé-Hart Instrument Co., Netcong, NJ).

Model fouling media characteristics are recorded in Table S-1. Model fouling media surface tensions were lower than that of water due to the presence of surfactants. The latex bead suspension surface tension was close to that of water, reflecting a relatively low surfactant concentration. As shown in Figure S - 1, the non-ionic Xiameter and Triton have 12 and 9.5 ethylene oxide units per molecule, respectively [27, 28].

According to their manufacturers, approximate critical micelle concentrations (CMC) of Xiameter and Triton surfactants are 0.02 wt% (200 ppm) and 0.22-0.24 mM (137-150 ppm), respectively [28]. Equilibrium surface tensions of saturated Xiameter and Triton aqueous solutions (1 wt%) are 26-28 and 33 dynes/cm, respectively [27, 29]. Surfactant concentrations in soybean and motor oil emulsions were below the surfactant's critical micelle concentrations, so the surface tension values of the emulsions were higher than the equilibrium surface tension values of the surfactants, but lower than that of pure water. The surface tension of the crude oil emulsion was lower than the equilibrium surface tension of Triton, suggesting that additional surface active ingredients were present in the crude oil. This finding is not surprising because crude oil commonly contains natural surface active agents [30].

Although these droplets were roughly similar in average size and concentration, their turbidities were not similar due to differences in the refractive indices of the latex beads and the various oils.

Table S-1. Model fouling media characteristics.

Characteristics	Suspension	Emulsions		
	Latex Beads	Soybean Oil	Motor Oil	Crude Oil
Surfactant(s)	Proprietary Non-ionic and ionic	Xiameter Non-ionic	Triton Non-ionic	Triton Non-ionic
Salt Concentration	0	0	1 wt%	0
Avg. Droplet Size [ $\mu\text{m}$ ]	4.0	3.4	3.9	3.4
Surface Tension [dynes/cm]	$71.9 \pm 2.4$	$70.8 \pm 2.7$	$47.8 \pm 3.5$	$26.3 \pm 1.1$
Zeta Potential [mV]	$-38.5 \pm 4.9$	$-22.2 \pm 0.8$	$-8.3 \pm 0.4$	$-20.0 \pm 1.3$
Turbidity [NTU]	501	221	103	93.8
Particle/oil Refractive Index	1.59*	1.4738	1.4802	1.4502
Particle/oil Density [ $\text{g}/\text{cm}^3$ ]	1.05*	0.92	0.87	0.77

\* Data provided by the manufacturer

### 3. MEMBRANE PURE WATER PERMEANCE CHARACTERIZATION

The pure water permeance of PVDF membranes was tested in UHP-76 stirred cells (Sterlitech, Kent, WA). The effective filtration area,  $A$ , was  $38.5 \text{ cm}^2$ . Ultrapure water was pressurized with compressed nitrogen on the upstream side of the membrane. The permeate was open to the atmosphere and was collected on a balance. The pressure difference between the upstream (i.e., feed) and downstream (i.e., permeate) faces of the membrane provided the TMP to drive water transport. The cumulative mass throughput,  $M$ , was recorded as a function of time,  $t$ , via LabVIEW<sup>®</sup> from National Instruments (Austin, TX). The pure water flux,  $J$ , was calculated as follows:

$$J = \frac{1}{\rho_{H_2O} A} \frac{dM}{dt} \quad [\text{S} - 1]$$

where  $\rho_{H_2O}$  is water density, and  $\frac{dM}{dt}$  is the steady state rate of water transport. The water permeance,  $P$ , is calculated by normalizing the pure water flux by TMP:

$$P = \frac{J}{TMP} \quad [S - 2]$$

#### 4. CONSTANT PERMEATE FLUX FOULING APPARATUS

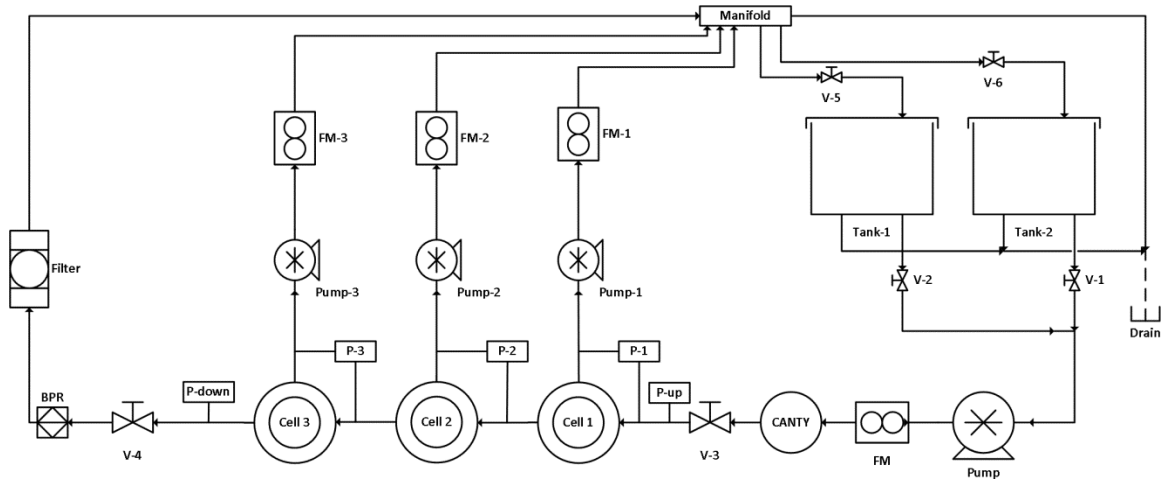


Figure S - 2. Constant permeate flux fouling system diagram. The two feed tanks, Tank-1 and Tank-2, were for ultrapure water and fouling media. The feed pump, Pump, was a gear pump. The feed flow meter (FM) was an oval gear flow meter. The inline particle analyzer (CANTY) was installed upstream of the membrane cells (Cell 1, Cell 2, Cell 3). Pressure transducers (P-up and P-down) measured the upstream and downstream pressure. Differential pressure transducers (P-1, P-2, P-3) measured the transmembrane pressure of each cell. The backpressure regulator (BPR) was connected to a compressed air cylinder, and it was operated in feedback control with P-up and P-down to maintain the feed side pressure of membranes. Peristaltic pumps (Pump-1, Pump-2, Pump-3) and Coriolis flow meters (FM-1, FM-2, FM-3) were installed on the permeate side of the membranes to maintain a constant permeate flux. The retentate and permeate were recycled to the feed tank. The cartridge filter was used to capture oil and particulates during system cleaning, and it is bypassed during filtration tests.